# The SIV Tilted Peptide Induces Cylindrical Reverse Micelles in Supported Lipid Bilayers†

Karim El Kirat,‡,§,|| Yves F. Dufrêne,§ Laurence Lins,‡ and Robert Brasseur*,‡

*Centre de Biophysique Moléculaire Numérique, Faculté Universitaire des Sciences Agronomiques de Gembloux, Passage des Déportés, 2, B-5030 Gembloux, Belgium, and Unité de chimie des interfaces, Université catholique de Louvain, Croix du Sud 2/18, B-1348 Louvain-la-Neuve, Belgium*

*Received February 15, 2006; Revised Manuscript Received May 31, 2006*

ABSTRACT: Elucidation of the molecular mechanism leading to biomembrane fusion is a challenging issue in current biomedical research in view of its involvement in controlling cellular functions and in mediating various important diseases. According to the generally admitted stalk mechanism described for membrane fusion, negatively curved lipids may play a central role during the early steps of the process. In this study, we used atomic force microscopy (AFM) to address the crucial question of whether negatively curved lipids influence the interaction of the simian immunodeficiency virus (SIV) fusion peptide with model membranes. To this end, dioleoylphosphatidylcholine/dipalmitoylphosphatidylcholine (DOPC/DPPC) bilayers containing 0.5 mol % dioleoylphosphatidic acid (DOPA) were incubated with the SIV peptide and imaged in real time using AFM. After a short incubation time, we observed a 1.9 nm reduction in the thickness of the DPPC domains, reflecting either interdigitation or fluidization of lipids. After longer incubation times, these depressed DPPC domains evolved into elevated domains, composed of nanorod structures protruding several nanometers above the bilayer surface and attributed to cylindrical reverse micelles. Such DOPC/DPPC/DOPA bilayer modifications were never observed with nontilted peptides. Accordingly, this is the first time that AFM reveals the formation of cylindrical reverse micelles in lipid bilayers promoted by fusogenic peptides.

Membrane fusion processes play an important role in controlling cell life (*1*−*3*) and in mediating infection processes (*1*). As bending of bilayers is necessary for the formation of intermediates during membrane fusion (*4*−*6*), negatively curved lipids (such as diglycerides, phosphatidylethanolamine, and phosphatidic acid) may be required. These lipids which cannot form bilayers preferentially organize as inverted micelles (*6*). Recent studies have shown that only very low concentrations (1−4 mol %) of such negatively curved lipids, which actually match physiological concentrations, are necessary for the promotion of membrane fusion (*6*). In cell membranes, these cone-shaped lipids are produced by the lipolytic activity of phospholipase C and D enzymes (PLC[1] and PLD, respectively). For example, PLD produces phosphatidic acid (PA) by hydrolyzing the phosphoester bond between the phosphatidyl moiety and the choline headgroup of phosphatidylcholine (PC). An important consequence of the production of PA by PLD is that it facilitates membrane fusion (*7*, *8*).

Negatively curved lipids are not the only promoters of membrane fusion since certain proteins and peptides also have the ability to induce membrane fusion processes that are biomedically important. For example, the role of viral fusion proteins is crucial for the internalization of the virus into host cells through a membrane fusion mechanism (*9*). Some neurodegenerative diseases (such as Alzheimer's and Creutzfeldt-Jakob diseases) are another example that illustrates peptide-induced perturbations of cell membranes (by the amyloid peptide and the prion protein, respectively). Hence, understanding the molecular basis of protein- and peptide-induced membrane fusion processes is challenging.

Tilted peptides are short peptides found in many membrane-interacting proteins (viral fusion proteins, neurotoxic proteins, lipolytic enzymes, etc.) (*10*). They are known to insert into lipid bilayers with an oblique orientation and to facilitate the formation of inverted micelles (*5*), thereby promoting membrane fusion processes. It has been suggested that the ability of tilted peptides to favor reverse micelle formation

† This work was supported by "Ministère de la Région Wallonne" Contract 0215103 (Nanomemb), the FNRS, the Université catholique de Louvain (Fonds Spéciaux de Recherche), and the Federal Office for Scientific, Technical and Cultural Affairs (Interuniversity Poles of Attraction Programme).

* To whom correspondence should be addressed: Centre de Biophysique Moléculaire Numérique, Faculté Universitaire des Sciences Agronomiques de Gembloux, Passage des Déportés, 2, B-5030 Gembloux, Belgium. Phone: (32) 81622521. Fax: (32) 81622522. E-mail: brasseur.r@fsagx.ac.be.

‡ Faculté Universitaire des Sciences Agronomiques de Gembloux.

§ Université catholique de Louvain.

|| Present address: UMR CNRS 6600, Biomécanique et Génie Biomédical, Université de Technologie de Compiègne, BP 20529, 60205 Compiègne Cedex, France.

[1] Abbreviations: AFM, atomic force microscopy; CPP, cell-penetrating peptide; DOPA, L-α-dioleoylphosphatidic acid; DOPC, L-α-dioleoylphosphatidylcholine; DPPC, L-α-dipalmitoylphosphatidylcholine; EDTA, ethylenediaminetetraacetic acid; gA, gramicidin A; MLV, multilamellar vesicles; PA, phosphatidic acid; PC, phosphatidylcholine; PL, phospholipids; PLC, phospholipase C; PLD, phospholipase D; SIV, simian immunodeficiency virus; SUV, small unilamellar vesicles; TFE, 2,2,2-trifluoroethanol.

10.1021/bi060317x CCC: $33.50 
Published on Web 07/01/2006

and fusion is more pronounced with negatively curved lipids (*5*, *10*, *11*). However, experimental data are still needed to gain a molecular picture of the interaction between tilted peptides and membranes.

Atomic force microscopy (AFM) has proven to be an efficient technique for imaging biological specimens at high resolution (*12*). AFM is very useful in biophysics in characterizing supported lipid bilayers at high resolution, in terms of formation of micro- and nanodomains (*13*, *14*) and of interaction with external agents, including solvents (*15*), peptides (*16*), proteins (*17*), and antibiotics (*18*). Furthermore, AFM aided in the study of many membranotropic peptides. For example, tapping mode AFM on the influenza hemagglutinin ectodomain provided evidence of its self-association when incorporated within membranes (*19*). Furthermore, as opposed to electron microscopy images, AFM images can be acquired under physiological conditions. This property allowed the elucidation of amylin-induced defects within supported membranes (*20*).

Here, we used AFM to elucidate the influence of negatively curved lipids on the ability of a viral fusion peptide to perturb the organization of lipid bilayers. The simian immunodeficiency virus (SIV) fusion peptide was selected because of its biomedical relevance and because it is known to destabilize lipid membranes (*21*−*25*). To probe the sensitivity of the SIV peptide toward curved lipids, mixed DOPC/DPPC bilayers containing 0.5% DOPA were imaged in the presence of the peptide. Real-time monitoring of the SIV peptide-induced modification of membrane topography provided novel information. We have noticed a significant reduction in the bilayer thickness of the DPPC domains after short incubation times with the peptide, while after longer times, the domains evolved toward a thicker phase.

## EXPERIMENTAL PROCEDURES

*Materials.* L-α-Dioleoylphosphatidic acid (DOPA), L-α-dioleoylphosphatidylcholine (DOPC), L-α-dipalmitoylphosphatidylcholine (DPPC), ethylenediaminetetraacetic acid (EDTA), and 2,2,2-trifluoroethanol were purchased from Sigma (St. Louis, MO). The SIV peptide ($NH_2$-GVFVLGFLGFLA-$CONH_2$) was obtained from Neosystem (Strasbourg, France) and was 90% pure. Other chemicals were purchased from Merck (Darmstadt, Germany). Stock solutions of peptides were prepared in trifluoroethanol (TFE) at a final concentration of 600 $\mu$M. For AFM experiments, stock solutions were diluted into Tris/EDTA buffer [10 mM Tris, 150 mM NaCl, and 5 mM EDTA (pH 7.4)] to a final peptide concentration of 10 $\mu$M.

*Preparation of Supported Lipid Bilayers.* Supported lipid bilayers were prepared using the vesicle fusion method (*13*, *26*). To this end, lipids were dissolved in chloroform at a final concentration of 1 mM. The mixture of these lipids was then evaporated under nitrogen and dried in a desiccator under vacuum for 2 h. Multilamellar vesicles (MLV) were obtained by resuspending the lipidic dried film in calcium-containing buffer [10 mM Tris, 150 mM NaCl, and 3 mM $CaCl_2$ (pH 7.4)] at a final lipid concentration of 1 mM. To obtain small unilamellar vesicles (SUV), the suspension was sonicated to clarity (four 2 min cycles) using a 500 W probe sonicator (Fisher Bioblock Scientific; 35% of the maximal power, 13 mm probe diameter) while keeping the suspension in an ice bath. The liposomal suspension was then filtered on 0.2 $\mu$m Nylon filters (Whatman Inc.) to eliminate titanium particles.

Freshly cleaved mica squares (16 $mm^2$) were glued onto steel sample disks (Veeco Metrology LLC, Santa Barbara, CA) using Epotek 377 (Gentec Benelux, Waterloo, Belgium). Two milliliters of the SUV suspension was then deposited onto the mica samples, and the SUV were allowed to adsorb and fuse onto the solid surface for 1 h at 60 °C. Subsequently, samples were rinsed five times with 2 mL of EDTA-containing buffer [10 mM Tris, 150 mM NaCl (pH 7.4), and 5 mM EDTA] and slowly cooled to room temperature.

*Atomic Force Microscopy.* Supported bilayers were investigated using a commercial AFM (NanoScope IV Multi-Mode AFM, Veeco Metrology LLC) equipped with a 125 $\mu$m × 125 $\mu$m × 5 $\mu$m scanner (J-scanner). Topographic images were recorded in contact mode using oxide-sharpened microfabricated $Si_3N_4$ cantilevers (Microlevers, Veeco Metrology LLC) with a spring constant of 0.01 N/m (manufacturer specified), with a minimal applied force (<500 pN) and at a scan rate of 5−6 Hz. Images were recorded at room temperature (23−25 °C) either in Tris/EDTA buffer [10 mM Tris, 150 mM NaCl, and 5 mM EDTA (pH 7.4)] or after incubation in Tris/EDTA buffer containing 10 $\mu$M peptide.

## RESULTS

To explore the sensitivity of tilted peptides for negatively curved lipids, mixed DOPC/DPPC/DOPA (495:500:5 molar ratio) bilayers were imaged by AFM in buffer solution in the absence and presence of the SIV peptide. As shown in Figure 1A (0 min), the topographic image obtained for a native DOPC/DPPC/DOPA bilayer revealed the coexistence of two phases, as observed for DOPC/DPPC-supported bilayers (*13*, *17*). The phase diagrams of DPPC and DOPC (*17*) as well as previous AFM studies (*17*, *18*) lead us to believe that the lighter level correspond to DPPC in the gel phase and the darker level to DOPC in the fluid phase. The step height measured between the two phases was 1.1 ± 0.1 nm and resulted from a difference in the thickness and mechanical properties of the DOPC and DPPC films (*13*, *27*). Importantly, we note that a third phase that can be attributed to PA-enriched domains was never seen in the images, presumably because the amount of PA (0.5 mol %) was too low to induce lateral segregation.

Addition of the SIV peptide to the DOPC/DPPC/DOPA bilayer induced profound, time-dependent modification of the bilayer morphology. Figure 1B shows that after incubation for 15 min, while the DOPC fluid phase remained apparently unchanged, the DPPC phase was depressed and exhibited a thickness reduction of 1.9 ± 0.1 nm. After 30 min (Figure 1C), elevated bright features protruding 3.2 ± 0.2 nm above the DOPC surface were observed. Since they appeared at the interface between the DOPC and the depressed DPPC phases, they are likely to represent a third, newly formed phase. Importantly, this elevated phase was found to grow with an increase in incubation time, in a centripetal way, from the edge of the DPPC-depressed domain toward its center (see panels D−H of Figure 1). Hence, incubation of DOPC/DPPC/DOPA bilayers with the SIV peptide induces two consecutive, marked morphological changes, i.e., depression of whole DPPC domains followed

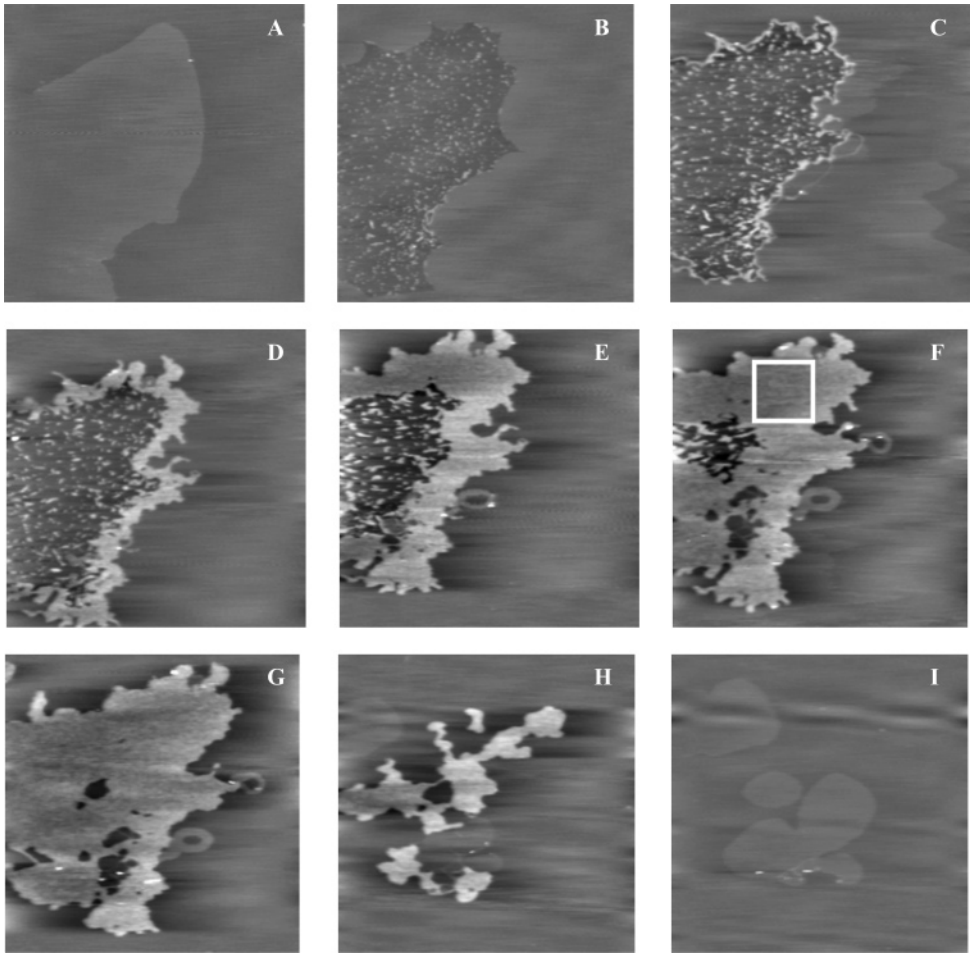


FIGURE 1: Influence of the SIV peptide on DOPC/DPPC/DOPA bilayers. AFM topographic images (15 $\mu$m × 15 $\mu$m, *z*-range of 10 nm) of a DOPC/DPPC/DOPA (495:500:5 molar ratio) bilayer recorded in Tris and EDTA (pH 7.4) (A, 0 min) and in a 10 $\mu$M SIV peptide solution (Tris/EDTA) after (B) 15, (C) 30, (D) 40, (E) 50, (F) 60, (G) 80, (H) 110, and (I) 120 min. These results are representative of four independent experiments with at least two different regions explored.

by the formation of a third elevated phase slowly covering the initial DPPC domain. Figure 2 is an enlargement of this newly generated domain corresponding to an incubation time of 60 min (corresponding to the white box in Figure 1F). As one can see, this new phase is composed of highly ordered tubular nanostructures with a periodicity of 77.4 ± 6.1 nm and an amplitude of 0.7 ± 0.1 nm.

From the AFM images depicted in Figure 1, we have measured the height difference between the new thick phase and the surrounding DOPC. The heights were then plotted as a function of incubation time. Importantly, we note that the newly formed phase became progressively thicker with time (Figure 3), the step height with respect to the unmodified DOPC phase increasing from 3.2 ± 0.2 nm at 30 min to 5.2 ± 0.4 nm at 110 min. In fact, the newly formed phase finally reached the thickness of a new bilayer deposited onto the native DOPC membrane.

At 110 min (Figure 1H), the elevated domain slowly desorbed from the bilayer, and at 120 min, it had completely disappeared, leaving round-shaped DPPC-like phases protruding 0.7 ± 0.1 nm from the DOPC surface. Importantly, at the end of the incubation, no domains enriched with the SIV peptide were visible, supporting the hypothesis of its complete desorption from the bilayer.

It is important to note that among the DOPA percentages that were tested (0.05, 0.5, 2, and 5 mol %), only the 0.5% DOPA-containing bilayers gave satisfactory results in terms of the velocity and intensity of the observed phenomena. Above this adequate percentage of 0.5% DOPA, the reaction evolved too fast to image every step with sufficient resolution. At <0.5% DOPA, the modifications of the membrane were too slow to observe the overall mechanism of the reaction (*11*).

Furthermore, it is worth noting that while other tilted peptides, such as prion peptide or colicin H8 and H9, also induced the formation of transiently thicker domains (data not shown), these were not observed with nontilted amphipathic peptide ApoE, as shown in Figure 4. Within 8 min of ApoE peptide addition (10 $\mu$M), an important part of the initial DPPC gel phase was depressed by 1.8 ± 0.2 nm. One can also notice that some round DPPC domains appeared. After 15 min, all the depressed domain disappeared, leaving round-shaped DPPC domains and some white aggregates protruding 0.9 ± 0.1 nm above DOPC (see the arrow in Figure 4C). According to the thickness and the low mechanical resistance of these aggregates, they may correspond to areas enriched with the ApoE peptide lying flat on the membrane. Thus, as opposed to the case for the SIV peptide, membrane modifications induced by the ApoE peptide occurred within 15 min and did not involve elevated domains. Therefore, interaction of the SIV peptide with the membrane

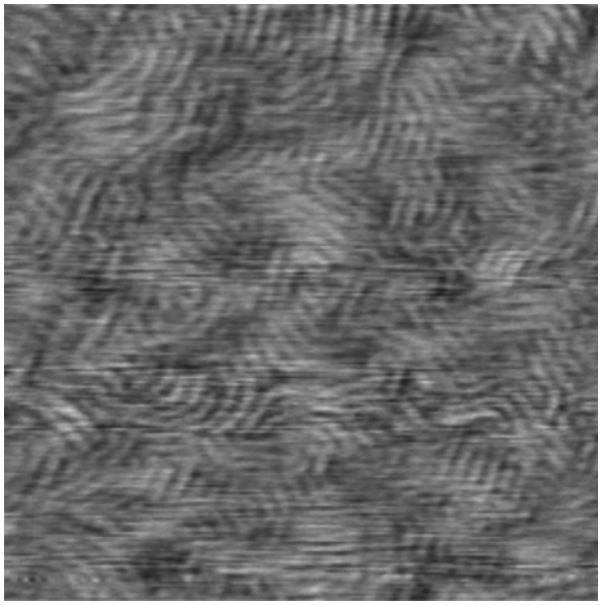

FIGURE 2: SIV peptide induces the formation of thick domains within DOPC/DPPC/DOPA bilayers. Higher magnification (3 $\mu$m $\times$ 3 $\mu$m, *z*-range of 2 nm) of the AFM topographic image shown in Figure 1F (white box). This image is representative of three independent experiments with at least two different regions explored.

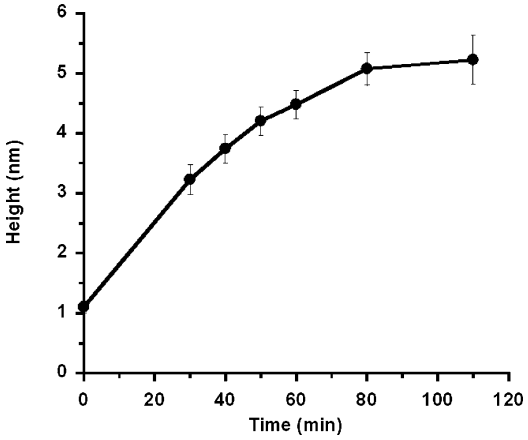


FIGURE 3: Evolution of the thickness of the newly formed phase induced by the SIV peptide. Step height differences were measured between the newly formed phase and the surrounding DOPC in the images presented in Figure 1. These heights were then plotted as a function of time.

appears to be quite different from that of the ApoE control peptide.

Fusion experiments were performed with 495:500:5 (molar ratio) DOPC/DPPC/DOPA liposomes with the protocol described previously (*28*). The results were very similar to those obtained for DOPC/DPPC bilayers (data not shown). This might be due to the low percentage of DOPA which was low enough to allow a detailed observation of the phenomena on a nanoscale, but it was not sufficient to significantly enhance the fusion of liposomes on a macroscale (*6*).

## DISCUSSION

Many transmembrane peptides have previously been studied by AFM. Synthetic WALP peptides were described in interaction with DPPC membranes (*29*). These α-helix

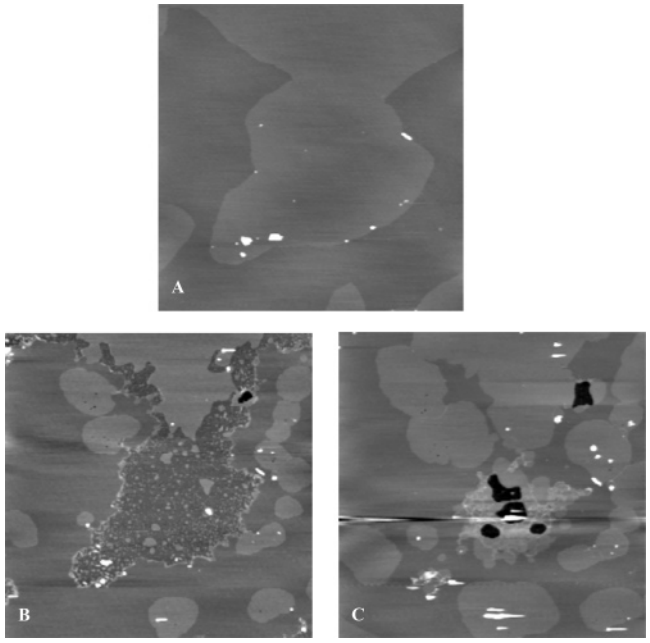


FIGURE 4: Influence of the ApoE peptide on DOPC/DPPC/DOPA bilayers. AFM topographic images (15 $\mu$m $\times$ 15 $\mu$m, *z*-range of 10 nm) of a DOPC/DPPC/DOPA (495:500:5 molar ratio) bilayer recorded in Tris and EDTA (pH 7.4) (0 min) and in a 10 $\mu$M ApoE peptide solution (Tris/EDTA) after 8 (B) and 15 min (C). These results are representative of two independent experiments with at least two different regions explored.

peptides formed stable striated domains corresponding to their transmembrane insertion. The authors also showed that the transmembrane line-type ordered arrangement of the peptide depended on its length. With the same protocol, the natural channel-forming peptide gramicidin A (gA) induced the formation of highly ordered domains composed of gA aggregates within DPPC bilayers (*30*). At higher gA concentrations, small clusters of elongated (line-type) aggregates appeared with reproducible segment lengths. An increasing gA ratio induced the formation of multiple lamellar structures on the DPPC bilayer with a ripplelike surface morphology resembling to some extent to the thick domains found here. A noteworthy fact is that due to the low resistance of this ripplelike structure, the top aggregate layer could be easily scraped away by applying a large force on the AFM tip, exposing the lower layer which appeared to be the same as those with low gA concentrations. This is very similar to what was observed here for the SIV peptide, when the elevated phase finally desorbed after long incubation times. In another recent work, Plénat et al. (*31*) demonstrated the coexistence of two states for a cell-penetrating peptide (CPP). The first form was composed of bundles of thin elongated well-delimited filaments lying at the surface of the lipid bilayer, while some peptides where localized deeply within the membrane. The latter situation corresponded to localized thinning of the membrane from 1.2 to 3.5 nm.

Accordingly, the SIV-induced striated domains reported here show some similarities to those found for the gA peptides and the CPP at high concentrations. However, there is a major methodological difference; bilayers were prepared from mixed lipid/gA (or lipid/CPP) vesicles, and the final bilayer systems were then imaged. By contrast, in this work, lipid bilayers were first prepared, and then their modification upon addition of the SIV peptide was visualized in real time

while the system evolved toward equilibrium. Even if the topographic characteristics of our nanorods are very similar to those previously described (striated organized domains or ripple phases), their dynamic evolution is an essential difference suggesting that they are not of the same nature.

In this paper, the interaction of the SIV tilted peptide with bilayers containing 0.5% PA provoked the formation of a new elevated phase composed of tubular structures. These nanorods were presumably produced by the self-association of many reverse cylinders of peptides and lipids in a hexagonal HII phase. Indeed, these reverse cylinders might expose the hydrophobic tails of phospholipids (PL) at their surface, so they might self-associate to minimize their interaction with the surrounding water (*32*). Thus, the length of the reverse cylinders would correspond to the periodicity of the thick phase, i.e., 77.4 ± 6.1 nm, with the cylinders having their main axis perpendicular to the main axis of the nanorods. This period is in agreement with some recent AFM data obtained with surfactants (*32*) clearly showing that cylindrical reverse micelles have a length in the range of 50−100 nm. Furthermore, this mechanism of self-association is very similar to the one observed previously for association of Alzheimer's $\beta$-amyloid peptide onto hydrophobic surfaces in the absence of lipids (*33*).

It is also important to note that nanorod formation caused by the SIV peptide was never seen on DOPC/DPPC bilayers devoid of DOPA (*28*), indicating they are associated with the presence of this lipid. Moreover, the same behavior was also observed with dioleoylphosphatidylethanolamine, another negatively curved lipid which is uncharged under neutral pH conditions while DOPA is anionic (*34*). This observation illustrates that the charge has no effect on SIV peptide-induced formation of nanorods; it is due only to the lipid shape.

In light of the data presented here as well as in a previous paper (*11*), the following mechanism may be proposed to explain the formation of the elevated domains caused by the SIV peptide in PA-containing membranes. The type of structure generated immediately after addition of the SIV peptide to PA-containing membranes (Figure 5A) consists of large areas with an ~1.9 nm depression presumably due to DPPC interdigitation and/or fluidization. This phenomenon could occur in the case of massive insertion of the SIV peptide as previously described for transmembrane peptides at high concentrations in PC bilayers (*29*). In such depressions, the amount of inserted peptide may be sufficiently high to alter the topographic characteristics of DPPC. Such a high surface density of peptides would make the membrane fragile. Therefore, one may expect an evolution of these depressions toward more stable structures. Indeed, DPPC domain depressions were slowly replaced by new periodic features (Figure 5B), increasingly protruding until they reach a thickness corresponding to two standing PL molecules (~5 nm). These periodic structures may be cylindrical inverted micelles of mixed PL/SIV peptide (Figure 5C). Because of their hydrophobicity, they might self-associate in nanorods (see Figure 5D) with a periodicity corresponding to the length of the reverse tubular micelles. Two observations support this view: (1) the slow transient apparition of the nanorods and (2) their rapid disappearance from the bilayer surface. This is in agreement with the speed characteristics described for HII phase growth (*5*). They finally desorbed from the bilayer surface presumably through conversion into spherical reverse micelles. Consequently, the native topography was recovered at the end of the reaction with apparently restored DPPC domains. The dynamic modification of the bilayer is the major evidence supporting the model of HII phase formation initiated by the SIV peptide. It is also important to note that the phenomena observed here with the SIV peptide (depression of the membrane, together with spontaneous evolution and then desorption) have never been described in the case of ripple phases and striated domains.

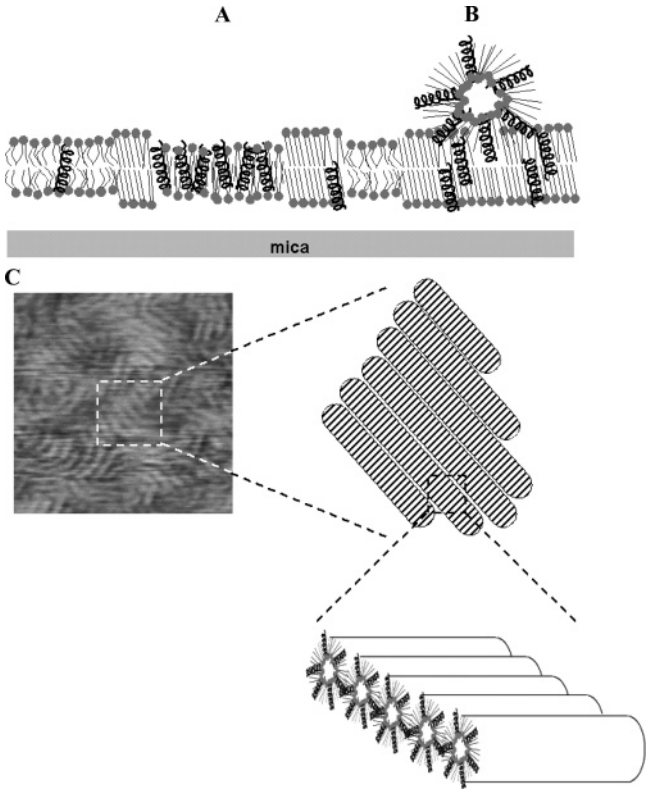


FIGURE 5: Schematic representation of SIV peptide-induced modification of PA-containing membranes. When the SIV peptide is added to 495:500:5 (molar ratio) DOPC/DPPC/DOPA bilayers, it inserts within the PL, leading to topographic modification of the surface. (A) A high concentration of inserted SIV peptide induced the formation of local depressions probably due to PL interdigitation and/or fluidization. (B) After a while, the depressed domains slowly evolved to protruding structures presumably composed of metastable cylindrical reverse micelles. They will eventually desorb to leave the surface with its native topography. (C) Schematic enlargement of the thicker phase showing that it is constructed, beginning with the smallest element, by self-association of cylindrical reverse micelles having their main axis perpendicular to the main axis of the nanorods that are visible in the AFM image. According to this model, cylindrical reverse micelles may present a length of 77.4 ± 6.1 nm, corresponding to the period of the thicker phase composed of nanorods. In this schematic representation, DOPA was not represented because its proportion was too low to induce visible lateral segregation in AFM images.

The presence of negatively curved lipids within membranes is often not sufficient to induce fusion. However, the insertion of peptides could provoke membrane destabilization leading to fusion. Therefore, fusion-triggering peptides may be more efficient when negatively curved lipids are initially present within the bilayer. Our AFM in situ images clearly demonstrated that negatively curved lipids are necessary to promote modifications of membrane phases and structures by the SIV peptide.

## ACKNOWLEDGMENT

L.L. and Y.F.D. are Research Associates of the Belgian National Foundation for Scientific Research (FNRS), and R.B. is Research Director of the FNRS.

## REFERENCES

1. Peuvot, J., Schanck, A., Lins, L., and Brasseur, R. (1999) Are the fusion processes involved in birth, life and death of the cell depending on tilted insertion of peptides into membranes? *J. Theor. Biol. 198*, 173−181.
2. Jena, B. P. (2004) Discovery of the Porosome: Revealing the molecular mechanism of secretion and membrane fusion in cells, *J. Cell. Mol. Med. 8*, 1−21.
3. Malinin, V. S., and Lentz, B. R. (2004) Energetics of vesicle fusion intermediates: Comparison of calculations with observed effects of osmotic and curvature stresses, *Biophys. J. 86*, 2951−2964.
4. Chernomordik, L. (1996) Non-bilayer lipids and biological fusion intermediates, *Chem. Phys. Lipids 81*, 203−213.
5. Epand, R. M., and Epand, R. F. (2000) Modulation of membrane curvature by peptides, *Biopolymers 55*, 358−363.
6. Haque, M. E., and Lentz, B. R. (2004) Roles of curvature and hydrophobic interstice energy in fusion: Studies of lipid perturbant effects, *Biochemistry 43*, 3507−3517.
7. Stieglitz, K. A., Seaton, B. A., and Roberts, M. F. (2001) Binding of proteolytically processed phospholipase D from *Streptomyces chromofuscus* to phosphatidylcholine membranes facilitates vesicle aggregation and fusion, *Biochemistry 40*, 13954−13963.
8. Blackwood, R. A., Smolen, J. E., Transue, A., Hessler, R. J., Harsh, D. M., Brower, R. C., and French, S. (1997) Phospholipase D activity facilitates $Ca^{2+}$-induced aggregation and fusion of complex liposomes, *Am. J. Physiol. 272*, C1279−C1285.
9. Hughson, F. M. (1997) Enveloped viruses: A common mode of membrane fusion? *Curr. Biol. 7*, R565−R569.
10. Brasseur, R. (2000) Tilted peptides: A motif for membrane destabilization (hypothesis), *Mol. Membr. Biol. 17*, 31−40.
11. El Kirat, K., Lins, L., Brasseur, R., and Dufrene, Y. F. (2005) Nanoscale Modification of Supported Lipid Membranes: Synergetic Effect of Phospholipase D and Viral Fusion Peptides, *J. Biomed. Nanotechnol. 1*, 39−46.
12. Engel, A., and Muller, D. J. (2000) Observing single biomolecules at work with the atomic force microscope, *Nat. Struct. Biol. 7*, 715−718.
13. Giocondi, M. C., Vie, V., Lesniewska, E., Milhiet, P. E., Zinke-Allmang, M., and Le Grimellec, C. (2001) Phase Topology and Growth of Single Domains in Lipid Bilayers, *Langmuir 17*, 1653−1659.
14. Reviakine, I., Bergsma-Schutter, W., Morozov, A. N., and Brisson, A. (2001) Two-Dimensional Crystallization of Annexin A5 on Phospholipid Bilayers and Monolayers: A Solid−Solid-Phase Transition between Crystal Forms, *Langmuir 17*, 1680−1686.
15. Mou, J., Yang, J., Huang, C., and Shao, Z. (1994) Alcohol induces interdigitated domains in unilamellar phosphatidylcholine bilayers, *Biochemistry 33*, 9981−9985.
16. Rinia, H. A., Boots, J. W., Rijkers, D. T., Kik, R. A., Snel, M. M., Demel, R. A., Killian, J. A., van der Eerden, J. P., and de Kruijff, B. (2002) Domain formation in phosphatidylcholine bilayers containing transmembrane peptides: Specific effects of flanking residues, *Biochemistry 41*, 2814−2824.
17. Milhiet, P. E., Giocondi, M. C., Baghdadi, O., Ronzon, F., Roux, B., and Le Grimellec, C. (2002) Spontaneous insertion and partitioning of alkaline phosphatase into model lipid rafts, *EMBO Rep. 3*, 485−490.
18. Berquand, A., Mingeot-Leclercq, M. P., and Dufrene, Y. F. (2004) Real-time imaging of drug-membrane interactions by atomic force microscopy, *Biochim. Biophys. Acta 1664*, 198−205.
19. Epand, R. F., Yip, C. M., Chernomordik, L. V., LeDuc, D. L., Shin, Y. K., and Epand, R. M. (2001) Self-assembly of influenza hemagglutinin: Studies of ectodomain aggregation by in situ atomic force microscopy, *Biochim. Biophys. Acta 1513*, 167−175.
20. Green, J. D., Kreplak, L., Goldsbury, C., Li, B. X., Stolz, M., Cooper, G. S., Seelig, A., Kistler, J., and Aebi, U. (2004) Atomic force microscopy reveals defects within mica supported lipid bilayers induced by the amyloidogenic human amylin peptide, *J. Mol. Biol. 342*, 877−887.
21. Martin, I., Dubois, M. C., Defrise-Quertain, F., Saermark, T., Burny, A., Brasseur, R., and Ruysschaert, J. M. (1994) Correlation between fusogenicity of synthetic modified peptides corresponding to the $NH_2$-terminal extremity of simian immunodeficiency virus gp32 and their mode of insertion into the lipid bilayer: An infrared spectroscopy study, *J. Virol. 68*, 1139−1148.
22. Voneche, V., Portetelle, D., Kettmann, R., Willems, L., Limbach, K., Paoletti, E., Ruysschaert, J. M., Burny, A., and Brasseur, R. (1992) Fusogenic segments of bovine leukemia virus and simian immunodeficiency virus are interchangeable and mediate fusion by means of oblique insertion in the lipid bilayer of their target cells, *Proc. Natl. Acad. Sci. U.S.A. 89*, 3810−3814.
23. Epand, R. F., Martin, I., Ruysschaert, J. M., and Epand, R. M. (1994) Membrane orientation of the SIV fusion peptide determines its effect on bilayer stability and ability to promote membrane fusion, *Biochem. Biophys. Res. Commun. 205*, 1938−1943.
24. Bradshaw, J. P., Darkes, M. J., Harroun, T. A., Katsaras, J., and Epand, R. M. (2000) Oblique membrane insertion of viral fusion peptide probed by neutron diffraction, *Biochemistry 39*, 6581−6585.
25. Lins, L., Charloteaux, B., Thomas, A., and Brasseur, R. (2001) Computational study of lipid-destabilizing protein fragments: Towards a comprehensive view of tilted peptides, *Proteins 44*, 435−447.
26. Reviakine, I., and Brisson, A. (2000) Formation of Supported Phospholipid Bilayers from Unilamellar Vesicles Investigated by Atomic Force Microscopy, *Langmuir 16*, 1806−1815.
27. Dufrene, Y. F., Barger, W. R., Green, J. B. D., and Lee, G. U. (1997) Nanometer-Scale Surface Properties of Mixed Phospholipid Monolayers and Bilayers, *Langmuir 13*, 4779−4784.
28. El Kirat, K., Lins, L., Brasseur, R., and Dufrene, Y. F. (2005) Fusogenic tilted peptides induce nanoscale holes in supported phosphatidylcholine bilayers, *Langmuir 21*, 3116−3121.
29. Rinia, H. A., Kik, R. A., Demel, R. A., Snel, M. M., Killian, J. A., Der Eerden, J. P., and de Kruijff, B. (2000) Visualization of highly ordered striated domains induced by transmembrane peptides in supported phosphatidylcholine bilayers, *Biochemistry 39*, 5852−5858.
30. Mou, J., Czajkowsky, D. M., and Shao, Z. (1996) Gramicidin A aggregation in supported gel state phosphatidylcholine bilayers, *Biochemistry 35*, 3222−3226.
31. Plenat, T., Boichot, S., Dosset, P., Milhiet, P. E., and Le Grimellec, C. (2005) Coexistence of a two-states organization for a cell-penetrating peptide in lipid bilayer, *Biophys. J. 89*, 4300−4309.
32. Nelson, M., Cain, N., Taylor, C. E., Ocko, B. M., Gin, D. L., Hammond, S. R., and Schwartz, D. K. (2005) Periodic Arrays of Interfacial Cylindrical Reverse Micelles, *Langmuir 21*, 9799−9802.
33. Kowalewski, T., and Holtzman, D. M. (1999) In situ atomic force microscopy study of Alzheimer's $\beta$-amyloid peptide on different substrates: New insights into mechanism of $\beta$-sheet formation, *Proc. Natl. Acad. Sci. U.S.A. 96*, 3688−3693.
34. Michaelson, D. M., Horwitz, A. F., and Klein, M. P. (1974) Head group modulation of membrane fluidity in sonicated phospholipid dispersions, *Biochemistry 13*, 2605−2612.

BI060317X